

The Milky Way’s rotation curve with superfluid dark matter

S. Hossenfelder,¹ T. Mistele^{1*}

¹Frankfurt Institute for Advanced Studies, Ruth-Moufang-Str. 1, D-60438 Frankfurt am Main, Germany

Accepted XXX. Received YYY; in original form ZZZ

ABSTRACT

Recent studies have shown that dark matter with a superfluid phase in which phonons mediate a long-distance force gives rise to the phenomenologically well-established regularities of Modified Newtonian Dynamics (MOND). Superfluid dark matter, therefore, has emerged as a promising explanation for astrophysical observations by combining the benefits of both particle dark matter and MOND, or its relativistic completions, respectively. We here investigate whether superfluid dark matter can reproduce the observed Milky Way rotation curve for $R < 25$ kpc and are able to answer this question in the affirmative. Our analysis demonstrates that superfluid dark matter fits the data well with parameters in reasonable ranges. The most notable difference between superfluid dark matter and MOND is that superfluid dark matter requires about 20% less total baryonic mass (with a suitable interpolation function). The total baryonic mass is then $5.96 \cdot 10^{10} M_{\odot}$, of which $1.03 \cdot 10^{10} M_{\odot}$ are from the bulge, $3.95 \cdot 10^{10} M_{\odot}$ are from the stellar disk, and $0.98 \cdot 10^{10} M_{\odot}$ are from the gas disk. Our analysis further allows us to estimate the radius of the Milky Way’s superfluid core (concretely, the so-called NFW and thermal radii) and the total mass of dark matter in both the superfluid and the normal phase. By varying the boundary conditions of the superfluid to give virial masses M_{200}^{DM} in the range $0.5 - 3.0 \cdot 10^{12} M_{\odot}$, we find that the NFW radius R_{NFW} varies between 65 kpc and 73 kpc, while the thermal radius R_T varies between about 67 kpc and 105 kpc. This is the first such treatment of a non-spherically-symmetric system in superfluid dark matter.

Key words: Galaxy: kinematics and dynamics – Galaxy: halo

1 INTRODUCTION

A naive combination of General Relativity and the matter-content of the Standard Model of particle physics does not correctly describe a variety of observations, ranging from the cosmic microwave background to galaxy clusters, to individual galaxies. The common remedy for this mismatch between theory and data is to conjecture a new type of matter – “dark matter” – which is presumably made of particles that so far evaded direct detection.

However, in the past two decades it has become increasingly clear that particle dark matter has its own problems, problems that are particularly obvious on galactic scales. A promising, alternative explanation for the puzzling astrophysical observations has been around since the mid 1980s. Its original formulation has become known as Modified Newtonian Dynamics (MOND) (Milgrom 1983a,b; Bekenstein & Milgrom 1984). The idea of MOND is simple: Instead of increasing the gravitational pull by adding a new type of

invisible matter, increase the gravitational pull of the normal matter by altering the force. For details, the reader is referred to the excellent reviews Sanders & McGaugh (2002) and Famaey & McGaugh (2012).

MOND is not relativistically invariant and non-local in the same way that Newtonian gravity is non-local. MOND therefore must be understood as an approximation that has to be completed to give a fully-relativistic theory of modified gravity. A variety of such relativistic completions of MOND have been proposed in the literature (Bekenstein 2004; Milgrom 2010; Zlosnik et al. 2007; Milgrom 2009; Deffayet et al. 2011; Blanchet & Heisenberg 2015; Hossenfelder 2017), but they face a common problem. While modifications of gravity are superior on galactic scales because of their parametric simplicity (Lelli et al. 2017), on larger scales dark matter is the simpler explanation. This tension between the cosmological and galactic scales can be resolved with any theory that combines cold dark matter for the former case and a MOND-limit for the latter. A very recent approach in this general direction is RelMOND (Skordis & Zlosnik 2020). An-

* E-mail: mistele@fias.uni-frankfurt.de

other strong contender for such a theory is superfluid dark matter (hereafter: SFDM) (Berezhiani & Khoury 2015).

The idea that dark matter may have a superfluid phase is itself not new (Sikivie & Yang 2009; Noumi et al. 2014; Davidson & Elmer 2013; de Vega & Sanchez 2014; Davidson 2015; Guth et al. 2015; Aguirre & Diez-Tejedor 2016; Dev et al. 2017; Eby et al. 2018; Sarkar et al. 2018), but the type of superfluid dark matter we are concerned with here is novel because it generates a long-range force. This force stems from the exchange of phonons between (effective) particles of normal matter and it reproduces the force-law of MOND. If the superfluid phase however breaks down – because the pressure is too low or the temperature too high – then the matter will behave like common-type particle dark matter. One then has to find a suitable type of particle for which a superfluid exists in galaxies, but not in intergalactic space or in the early universe.

It was shown in Berezhiani & Khoury (2015); Berezhiani et al. (2018) that one can combine the successes of MOND on galactic scales with the successes of Λ CDM on cosmological scales by choosing an axion-like particle with a mass in the range of $\approx 1\text{eV}$. Besides the mass of the particle, the free parameters of this model are the self-interaction strength of the new particle (which has to generate a superfluid) and the strength of its interaction with baryonic matter. We know from the observation of a gravitational wave event with an electromagnetic counterpart (Abbott et al. 2017) that the coupling of the superfluid to photons must be very small and we will therefore here set it to zero.

This SFDM is still young and how well it will fare for large-scale structure formation is not presently known. It has been shown however that superfluid dark matter can correctly reproduce rotation curves for a large variety of galaxies by the same mechanism that MOND does. For the same reason this model can explain the Tully-Fisher relation. In Hossenfelder & Mistele (2019) it was furthermore demonstrated the SFDM has no difficulties reproducing both the strong gravitational lensing data and the kinematic measurements for stellar rotation.

The aim of the present work is to see whether SFDM can give a reasonable Milky Way rotation curve and, more generally, to gain a qualitative understanding of SFDM in axisymmetric situations. The rotation curve of the Milky Way in an axisymmetric approximation was previously discussed in Lisanti et al. (2019a). Here, we add to this a detailed comparison between SFDM, its idealized MOND limit, and the Radial Acceleration Relation in MOND. We also, for the first time, estimate the superfluid core’s size and the virial dark matter mass of an axisymmetric system in SFDM. A statistically rigorous analysis of the goodness of fit of SFDM versus modified gravity and standard cold dark matter for the Milky Way rotation curve is beyond the scope of the present work. Given the qualitative agreement of the SFDM rotation curve with data that we will find below, such a study in isolation would anyway not be very informative. Instead, one would have to take into account all available astrophysical constraints on the model’s parameters. The work presented here shows how the Milky-Way analysis could be done as part of a global fit that takes into account the superfluid core’s finite size.

This paper is organized as follows. In Section 2 we briefly summarize the key properties of superfluid dark mat-

ter and recall its relation to MOND. In Section 3 we explain what data we are using. In Section 4 we detail how we integrate the equations and match them to the data. Results are presented in section 5. After a short discussion in Section 6 we conclude in Section 7.

2 SUPERFLUID DARK MATTER

Following the notation of Berezhiani & Khoury (2015), we describe the superfluid by a massive scalar field with phase θ . In the condensed phase the field associated with the phase is to good approximation classical. In the non-relativistic limit, the equations for the condensate are then (Berezhiani et al. 2018; Hossenfelder & Mistele 2018):

$$\Delta \left(-\frac{\hat{\mu}}{m} \right) = 4\pi G \left(\rho_b + \rho_{\text{SF}} \left(\hat{\mu}, (\vec{\nabla}\theta)^2 \right) \right), \quad (1a)$$

$$\vec{\nabla} \left(\frac{(\vec{\nabla}\theta)^2 + 2m(\frac{2\beta}{3} - 1)\hat{\mu}}{\sqrt{(\vec{\nabla}\theta)^2 + 2m(\beta - 1)\hat{\mu}}} \vec{\nabla}\theta \right) = \frac{\alpha}{2M_{\text{Pl}}} \rho_b, \quad (1b)$$

where

$$\rho_{\text{SF}} \left(\hat{\mu}, (\vec{\nabla}\theta)^2 \right) = \frac{2\sqrt{2}}{3} m^{5/2} \Lambda \frac{3(\beta - 1)\hat{\mu} + (3 - \beta) \frac{(\vec{\nabla}\theta)^2}{2m}}{\sqrt{(\beta - 1)\hat{\mu} + \frac{(\vec{\nabla}\theta)^2}{2m}}}. \quad (2)$$

Here, ρ_{SF} is the energy-density of the superfluid and ρ_b is the energy-density of baryons whose profile we extract from data as described in Sec. 3. m is the mass of the superfluid’s constituent particles, and $\hat{\mu} = \mu_{\text{nr}} - m\phi_{\text{N}}$ is a combination of the non-relativistic chemical potential μ_{nr} (a constant that acts as initial value) and the Newtonian gravitational potential ϕ_{N} . Expressed in these terms, Eq. (1a) is the usual Poisson equation for the Newtonian gravitational potential and Eq. (1b) determines SFDM’s phonon field θ that carries the MOND-like force.

In the above equations, M_{Pl} denotes the Planck mass, α is a dimensionless coupling constant, and Λ is related to the self-interaction strength of the new field (Berezhiani & Khoury 2015). The parameter β quantifies finite-temperature corrections as discussed in Berezhiani & Khoury (2015).

In SFDM, the baryons’ total acceleration \vec{a}_{tot} is then a sum of the acceleration from the Newtonian gravitational pull due to the baryonic and superfluid mass densities, \vec{a}_{N} , and the acceleration from the phonon force, \vec{a}_{θ} , which is proportional to the gradient $\vec{\nabla}\theta$:

$$\vec{a}_{\text{tot}} = \vec{a}_{\text{N}} + \vec{a}_{\theta} = -\vec{\nabla}\phi_{\text{N}} - \frac{\alpha\Lambda}{M_{\text{Pl}}} \vec{\nabla}\theta. \quad (3)$$

In our below analysis, we will further consider an idealized MOND-limit to highlight the differences between the two models. In this MOND-limit, we neglect the energy-density of the superfluid and assume that the kinetic energy of the phonon field is much larger than the chemical potential $|\vec{\nabla}\theta|^2/(2m) \gg \hat{\mu}$. In this case, the equations simplify to

$$\Delta\phi_{\text{N}} = 4\pi G \rho_b, \quad (4a)$$

$$\vec{\nabla} \left(\left(\frac{\sqrt{(\vec{\nabla}\theta)^2}}{a_{0,\theta}} \right) \vec{\nabla}\theta \right) = 4\pi G \rho_b, \quad (4b)$$

where we introduced the parameters $\bar{\theta} = (\alpha\Lambda/M_{\text{Pl}})\theta$, $a_{0,\theta} = \alpha^3\Lambda^2/M_{\text{Pl}}$, and $8\pi G = M_{\text{Pl}}^{-2}$ to match the expressions to the common MOND-formalism.

MOND further requires an interpolation function whose purpose is to fade out the regime of Newtonian gravity and cross over to the new, logarithmic potential law. This interpolation function is defined as the scalar function that, when multiplied with the acceleration from the Newtonian gravitational pull of the normal matter gives the total acceleration in MOND. This interpolation function corresponds to the phenomenologically obtained Radial Acceleration Relation (RAR)¹. Strictly speaking, this is correct only in the no-curl approximation, see Section 4. However, we show in Section 5.1 that the no-curl approximation is good to use, and hence the use of the radial acceleration relation justified.

An interpolation function is not necessary in SFDM, but to compare our results to those obtained with MOND, we use the exponential MOND interpolation function

$$\nu_e(y) = \frac{1}{1 - e^{-\sqrt{y}}}, \quad (5)$$

where $y = a_b/a_{0,e}$ with the Newtonian baryonic acceleration a_b and the acceleration scale $a_{0,e} = 1.2 \cdot 10^{-10} \text{ m/s}^2$.

As laid out in Hossenfelder & Mistele (2018), in the idealized MOND-limit, SFDM is equivalent to MOND with the interpolation function

$$\nu_\theta(y) = 1 + \frac{1}{\sqrt{y}}, \quad (6)$$

where $y = a_b/a_{0,\theta}$ and the acceleration scale is $a_{0,\theta} = 0.87 \cdot 10^{-10} \text{ m/s}^2$ for the fiducial parameter values from Berezhiani et al. (2018). Again, this equivalence strictly speaking only holds in the no-curl-approximation, because the curl-terms in the SFDM model are different from those of MOND even in the idealized MOND-limit. However, as we will see later, the difference is negligible for fitting the data we will be dealing with. In the non-idealized case, SFDM cannot be cast into the form of an interpolation function both because of the superfluid's gravitational pull and because the phonon force is not exactly of the MOND form.

3 DATA

Recently, McGaugh (2019) put forward a new model for the Milky Way (MW) to match the most up-to-date terminal velocity data. It provides an excellent fit to the MW's rotation curve even outside the range where this model was fitted. This model relates the Newtonian acceleration from the baryonic mass distribution with the total acceleration by employing the Radial Acceleration Relation from Lelli et al. (2017).

We take the baryonic mass distribution from McGaugh (2019) with a few minor modifications. Our model consists of a bulge, a gas disk, and a stellar disk. We take the stellar disk exactly as in McGaugh (2019), i.e. we use a scale height of 300 pc with the numerical surface density from McGaugh (2019). For the gas disk, we also use the numerical surface

density from McGaugh (2019). However, following Bovy & Rix (2013), we use a disk with scale height 130 pc instead of an infinitely thin disk because a finite height is easier to handle with our numerical code. The choice of this scale height does not significantly affect our results.

The gas surface density is that of Olling & Merrifield (2001), but scaled up by a factor of 1.4 to account for helium and metals, and adjusted for newer measurements of the Galactic size R_0 (Gravity Collaboration 2018), see McGaugh (2008, 2019) for details. This value of R_0 is a little outdated and a newer value was provided in Gravity Collaboration et al. (2019). However, since the exact value does not affect our conclusions much we just reuse the model from McGaugh (2019) with the therein used value. The resulting gas surface density in this model is not a smooth exponential. The stellar surface density is based on a Freeman Type II profile (Freeman 1970) that was adjusted to fit the detailed terminal velocity data for $3 \text{ kpc} < R < 8 \text{ kpc}$, see McGaugh (2019).

The bulge profile is parameterized as McGaugh (2008)

$$\rho_{\text{bulge}}(b) = \frac{\rho_{\text{bulge},0}}{\eta\zeta b_m^3} \frac{\exp[-(b/b_m)^2]}{(1 + b/b_0)^{1.8}}, \quad (7)$$

where $\eta = 0.5$, $\zeta = 0.6$, $b_m = 1.9 \text{ kpc}$, $b_0 = 0.1 \text{ kpc}$, and $b = r/(\eta\zeta)^{1/3}$ with the spherical radius r . This is the spherically equivalent mass distribution of the triaxial model used in McGaugh (2019). The constant $\rho_{\text{bulge},0}$ is chosen such that the asymptotic Newtonian acceleration due to the bulge is the same as in McGaugh (2019), see Table 2 there.

In the following, we keep the shape of the baryonic mass distribution fixed, but allow to rescale the baryonic mass distribution as a whole in order to fit the MW rotation curve. For this, we introduce the parameter f_b that multiplies the baryonic mass distribution $\rho_b(R, z)$. Here, R and z are the usual cylindrical coordinates.

We take the MW rotation curve data from McGaugh (2019). That is, we take the rotation curve data from Eilers et al. (2019) for $R > 5 \text{ kpc}$ and from Portail et al. (2017) for $R < 2.2 \text{ kpc}$, but with two adjustments made in McGaugh (2019): The Jeans analysis in Eilers et al. (2019) assumes a smooth exponential stellar profile. Therefore, McGaugh (2019) has redone the analysis of Eilers et al. (2019) with the profile described above. Also, McGaugh (2019) has scaled the radii of Portail et al. (2017) to be consistent with the newer measurement of R_0 from Gravity Collaboration (2018). Rescaling the total baryonic mass with our parameter f_b does not require redoing the analysis from Eilers et al. (2019), since the normalization cancels out, see e.g. their Eq. (3). Therefore, we can adjust the total baryonic mass while keeping the same rotation curve data.

4 METHOD AND DATA ANALYSIS

4.1 The Rotation Curve

Equations (1a) and (1b) describe only the core of the superfluid in the galactic center, not the non-superfluid phase at larger radii. However, our later estimate (see Section 5.3) shows that all data points fall well inside the superfluid core so that Eqs. (1a) and (1b) are sufficient to calculate the MW rotation curve in SFDM. As numerical values for the

¹ We wish to emphasize that with Radial Acceleration Relation we refer to the relation between the radial accelerations in general, not to the fit of this relation with a specific interpolation function.

parameters in Eqs. (1a) and (1b) we use the fiducial values from [Berezhiani et al. \(2018\)](#): $\beta = 2$, $\alpha = 5.7$, $m = 1 \text{ eV}$, and $\Lambda = 0.05 \text{ meV}$.

To integrate the equations, we assume axisymmetry and, as usual, parameterize it with cylindrical coordinates (R, z) . We calculate the rotation curve $v_c(R)$ as

$$v_c(R) = \sqrt{R \cdot |a_{\text{tot},R}(R, z=0)|}, \quad (8)$$

where $a_{\text{tot},R}$ is the R -component of the total acceleration \vec{a}_{tot} . In the case of the full SFDM equations we use the boundary conditions

$$\partial_z \hat{\mu}|_{z=0} = 0, \quad (9a)$$

$$\partial_z \theta|_{z=0} = 0, \quad (9b)$$

$$\hat{\mu}|_{\sqrt{R^2+z^2}=r_\infty} = \mu_\infty, \quad (9c)$$

$$\theta|_{\sqrt{R^2+z^2}=r_\infty} = 0. \quad (9d)$$

The first two conditions encode the $z \rightarrow -z$ symmetry, the other two conditions impose spherical symmetry at r_∞ . This approximation of spherical symmetry is a good approximation in MOND and Newtonian gravity ([Milgrom 1986](#)) which makes it reasonable that it is a good approximation here too.

For θ , the numerical value at r_∞ does not enter our equations so we just set it to zero. For $\hat{\mu}$, the numerical value at r_∞ determines the superfluid's density and therefore the superfluid's gravitational pull. This gravitational pull is typically subdominant in the inner regions of a galaxy, but it is important at larger radii, e.g. to produce enough strong lensing ([Hossenfelder & Mistele 2018](#)). Here, we choose the fixed value $\mu_\infty/m = 1.25 \cdot 10^{-8}$ at $r_\infty = 100 \text{ kpc}$. As we will see below, this gives a subdominant but non-negligible contribution to the rotation curve at $R < 25 \text{ kpc}$. Other choices of μ_∞/m and r_∞ are discussed in Sec. 5.4.

For the idealized MOND limit, we impose the boundary conditions

$$\partial_z \phi_N|_{z=0} = 0, \quad (10a)$$

$$\partial_z \bar{\theta}|_{z=0} = 0, \quad (10b)$$

$$\phi_N|_{\sqrt{R^2+z^2}=r_\infty} = 0, \quad (10c)$$

$$\bar{\theta}|_{\sqrt{R^2+z^2}=r_\infty} = 0. \quad (10d)$$

Since in this limit we neglect the superfluid's energy density ρ_{SF} , the numerical value of ϕ_N and $\bar{\theta}$ do not enter the equations and we can set both to zero.

Eqs. (4b) and (1b) are of the form $\vec{\nabla}(g \vec{\nabla} \theta) = 4\pi G \rho_b$ with some function g . Therefore, they can be written as $\vec{\nabla}(g \vec{\nabla} \theta - \vec{\nabla} \phi_{N,b}) = 0$, where $\phi_{N,b}$ is the Newtonian gravitational potential produced by the baryons. This gives $g \vec{\nabla} \theta = \vec{\nabla} \phi_{N,b}$ up to a term that can be written as the curl of a vector field. Neglecting this term is often a reasonable approximation ([Brada & Milgrom 1995](#)). Below, we will refer to this approximation as the 'no-curl-approximation' and investigate how good an approximation to the full equations it is.

A summary of the numerical parameters used in the present work is shown in Table 1. For more details on our numerical analysis, please refer to Appendix A.

Table 1. The numerical parameters used in the present work. We keep the model parameters fixed at the fiducial values from [Berezhiani et al. \(2018\)](#). The baryonic density is fixed up to an overall factor f_b , various values of which are discussed in Sec. 5.1 and Sec. 5.2. The boundary conditions for the superfluid are kept fixed in Sec. 5.1 and Sec. 5.2 but are varied in Sec. 5.4.

Model parameters		
m	1 eV	from Berezhiani et al. (2018)
α	5.7	from Berezhiani et al. (2018)
Λ	0.05 meV	from Berezhiani et al. (2018)
β	2	from Berezhiani et al. (2018)
Baryonic mass		
Bulge	$1.29 \cdot 10^{10} M_\odot \times f_b$	see Eq. (7)
Stellar disk	$4.94 \cdot 10^{10} M_\odot \times f_b$	from McGaugh (2019)
Gas disk	$1.22 \cdot 10^{10} M_\odot \times f_b$	from McGaugh (2019)
f_b	0.8	unless stated otherwise
Boundary condition		
μ_∞/m	$1.25 \cdot 10^{-8}$	unless stated otherwise
r_∞	100 kpc	unless stated otherwise

4.2 The Size of the Superfluid Core

[Berezhiani et al. \(2018\)](#) gives two different methods to estimate the size of the superfluid core for the case of spherical symmetry. The first method uses the so-called thermal radius R_T , the second method uses the so-called NFW radius R_{NFW} . Here, we will generalize both methods to axisymmetric situations. This will allow us to estimate the size of the superfluid's core in the R -direction ($R_{T,R}$ and $R_{\text{NFW},R}$) and in the z -direction ($R_{T,z}$ and $R_{\text{NFW},z}$). Both methods will make use of the fact that the superfluid core is approximately spherically symmetric at large radii, although it is only axially symmetric at smaller radii.

We start with the thermal radius R_T . According to Sec. III of [Berezhiani et al. \(2018\)](#) this radius is determined by the relation

$$\Gamma = t_{\text{dyn}}^{-1}, \quad (11)$$

where Γ is the local self-interaction rate and t_{dyn} is the dynamical time. Here, $\Gamma = (\sigma/m) \mathcal{N} v \rho$, where σ is the self-interaction rate, $\mathcal{N} = (\rho/m)(2\pi/mv)^3$ is the Bose-degeneracy factor, and v is the average velocity of the particles. As in [Berezhiani et al. \(2018\)](#), we take $\sigma/m = 0.01 \text{ cm}^2/\text{g}$.

The assumption of spherical symmetry enters in the calculation of t_{dyn} and v . Specifically, [Berezhiani et al. \(2018\)](#) takes $t_{\text{dyn}} \approx r/v$ and $v^2 \approx r \partial_r \phi_N$ with the spherical radius r . For axisymmetric situations, we adjust this to be $t_{\text{dyn}} \approx R/v|_{z=0}$ and $v^2 \approx R \partial_R \phi_N|_{z=0}$ for the thermal radius $R_{T,R}$ in R -direction and $t_{\text{dyn}} \approx z/v|_{R=0}$ and $v^2 \approx z \partial_z \phi_N|_{R=0}$ for the thermal radius $R_{T,z}$ in z -direction.

To estimate the NFW radius R_{NFW} , one assumes a superfluid in the centers of galaxies followed by an NFW profile at larger radii. The NFW radius R_{NFW} is then the radius at which the density and pressure of the superfluid core can be matched to the density and pressure of an NFW halo. Since the standard NFW profile is by definition spherically symmetric, the NFW radius is well-defined only when the

superfluid core is spherically symmetric as well at the radius R_{NFW} . In our case, the superfluid will not be exactly spherically symmetric. However, the superfluid is approximately spherically symmetric at the NFW radius, if this radius is large enough. Thus, we define $R_{\text{NFW},R}$ to be the value of R at $z = 0$, where the superfluid's density and pressure match those of the NFW halo, and $R_{\text{NFW},z}$ to be the value of z at $R = 0$ where the pressure and density match. If the superfluid is approximately spherically symmetric at the NFW radii defined in this way, we will have $R_{\text{NFW},R} \approx R_{\text{NFW},z}$. The formulas for the pressure and density of the superfluid and the NFW halo can be taken directly from [Berezhiani et al. \(2018\)](#).

5 RESULTS

5.1 Results for the idealized MOND regime

We begin with the results for the idealized MOND-limit of superfluid dark matter. The free parameter in this fit, f_b , is a factor for rescaling the total mass of baryons. In [McMillan \(2017\)](#); [Licquia & Newman \(2015\)](#) the stellar mass in the Milky Way was estimated with an observational uncertainty in the range of 10 – 20%. We therefore expect that the total mass of baryons has a similar observational uncertainty, which justifies allowing f_b to vary by this amount.

Fig. 1 shows the rotation curve of the Milky Way in terms of v_c from Eq. (8) in the MOND-limit in comparison with data for $f_b = 0.9, 0.8$, and 0.7 . The rotation curve data in this figure is that from [Eilers et al. \(2019\)](#) and [Portail et al. \(2017\)](#) adjusted to match the assumptions of [McGaugh \(2019\)](#), as described in Sec. 3.

As one sees, to obtain a reasonable fit of the rotation curve data in the idealized MOND-limit of SFDM, we need 10 – 20% less baryonic mass than the model of [McGaugh \(2019\)](#), i.e. $f_b \approx 0.8 - 0.9$. For $f_b = 0.8$, the total stellar mass in our model is $M_* = 4.98 \cdot 10^{10} M_\odot$. [McMillan \(2017\)](#) estimates the MW's total stellar mass as $(5.43 \pm 0.57) \cdot 10^{10} M_\odot$ and [Licquia & Newman \(2015\)](#) estimates $(6.08 \pm 1.14) \cdot 10^{10} M_\odot$. Thus, our value for M_* is relatively low, but still falls inside the error bars of [McMillan \(2017\)](#); [Licquia & Newman \(2015\)](#).

We have checked that with the ν_e interpolation function and the no-curl-approximation for $f_b = 1$, our calculation reproduces the results shown in Fig. 3 of [McGaugh \(2019\)](#) up to numerical differences and the minor modifications described in Sec. 3.

There are three differences between SFDM's idealized MOND regime and the RAR as applied in [McGaugh \(2019\)](#). First, the shapes of the interpolation functions ν_θ and ν_e differ. Second, the acceleration scales $a_{0,\theta}$ and $a_{0,e}$ differ. And third, [McGaugh \(2019\)](#) uses the no-curl-approximation while SFDM's idealized MOND-regime does not.

We have found that using the no-curl-approximation induces a non-negligible error only at $R \lesssim 5$ kpc. But even at $R \lesssim 5$ kpc, this error is only a few percent on v_c . Thus, the no-curl-approximation is not the main reason SFDM's idealized MOND regime requires significantly less baryonic mass than the ν_e -based model from [McGaugh \(2019\)](#).

The effect of the different acceleration scales $a_{0,\theta}$ and $a_{0,e}$ can be seen by using $a_{0,e}$ instead of $a_{0,\theta}$ in the equations of SFDM's idealized MOND regime. This is shown in

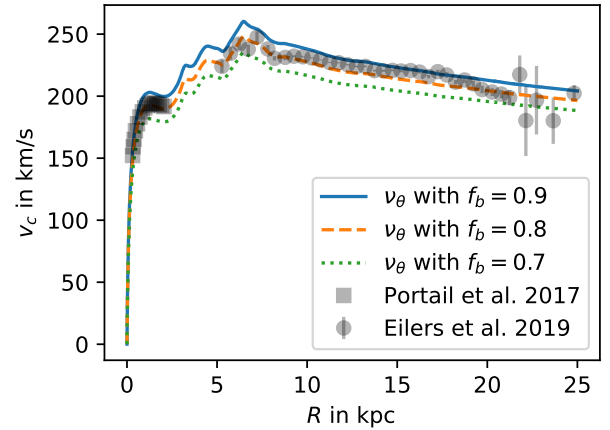


Figure 1. Milky Way rotation curve in the idealized MOND-limit of SFDM for different values of f_b . Also shown are the data from [Eilers et al. \(2019\)](#) (black dots) and [Portail et al. \(2017\)](#) (black squares), both adjusted to match the assumptions of [McGaugh \(2019\)](#).

Fig. 2. The effect of using $a_{0,e}$ instead of $a_{0,\theta}$ is larger at larger radii, where the additional MOND-like force begins to dominate. There, the larger acceleration scale increases v_c . Thus, the smaller acceleration scale $a_{0,\theta}$ helps SFDM's idealized MOND-limit to not require even less mass to fit the MW rotation curve.

This leaves the shape of ν_θ as the main reason that SFDM's idealized MOND regime requires less baryonic mass than the model from [McGaugh \(2019\)](#). Concretely, ν_e approaches 1 at large baryonic accelerations much faster than ν_θ . Therefore, at large and intermediate accelerations, ν_θ produces a larger total acceleration than ν_e . As a result, less baryonic mass is needed to match the rotation curve data.

From Fig. 2 we can further see that SFDM's idealized MOND regime produces rotation curves not only with a different normalization compared to the model from [McGaugh \(2019\)](#), but also with a different shape. This is a consequence of both the different interpolation functions ν_e and ν_θ and the different acceleration scales $a_{0,\theta}$ and $a_{0,e}$. Below, we will see that the full SFDM equations can produce rotation curves that are closer to that of the ν_e -based model from [McGaugh \(2019\)](#).

The above results for SFDM's idealized MOND-limit may also apply to Covariant Emergent Gravity (CEG) ([Hossenfelder 2017](#)) because CEG reduces to the same equations as SFDM's idealized MOND-limit, if we assume that only the 0-component of CEG's vector field u^μ is nonzero ([Hossenfelder & Mistele 2018](#)). However, it is not clear whether or not this assumption holds for axisymmetric systems like the MW. Also, the numerical value of the acceleration scale may be different for CEG, see [Hossenfelder & Mistele \(2018\)](#). Thus, one should be careful when applying the above results to CEG.

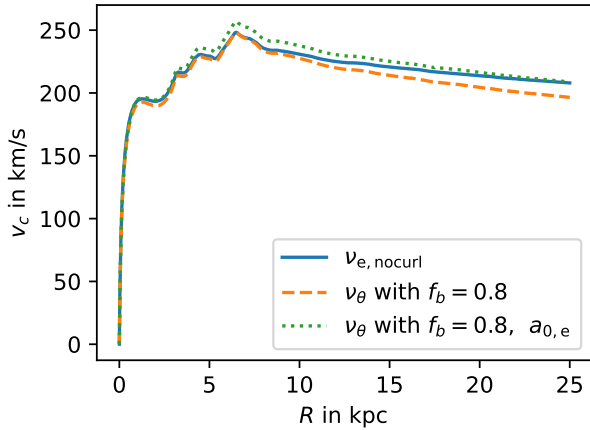


Figure 2. Top: Milky Way rotation curve in the idealized MOND regime of SFDM for $f_b = 0.8$ (dashed orange line), with $f_b = 0.8$ and $a_{0,e}$ instead of $a_{0,\theta}$ (dotted green line) compared with the ν_e rotation curve with $f_b = 1$ (solid blue line).

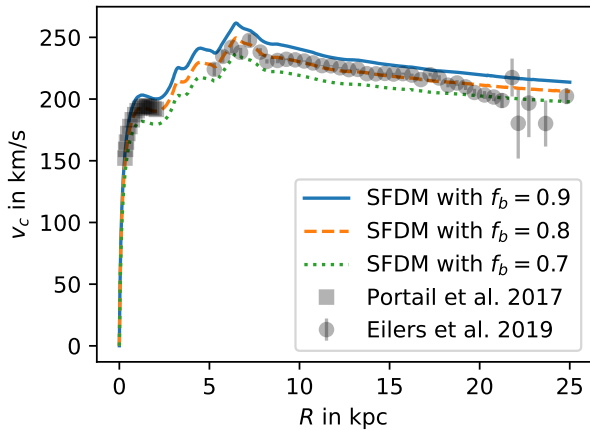


Figure 3. SFDM MW rotation curve for $f_b = 0.9$ (blue line), $f_b = 0.8$ (dashed orange line), and $f_b = 0.7$ (dotted green line). Also shown are the data from Eilers et al. (2019) (black dots) and Portail et al. (2017) (black squares), both adjusted to match the assumptions of McGaugh (2019).

5.2 Results for full SFDM

Fig. 3 compares the data of the Milky-Way rotation curve to the results from the full equations of superfluid dark matter. Again we have plotted the results for different values of the total mass of baryons, $f_b = 0.7, 0.8$, and 0.9 . As one sees, we get a good fit for f_b around 0.8 , which is similar to our finding for the idealized MOND-limit discussed in the previous subsection.

This is not a trivial consequence of the results from the realized MOND limit because now the superfluid’s gravitational pull also contributes to the rotation curve. This gravitational pull can change both the shape and the normalization of the rotation curve. In our case, the superfluid’s gravitational pull has a significant effect on the shape of the

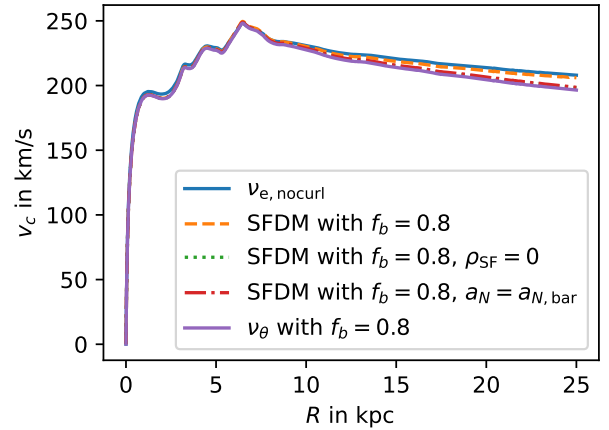


Figure 4. MW rotation curve from the ν_e -based model from McGaugh (2019) (solid blue line), from SFDM with $f_b = 0.8$ (dashed orange line), from SFDM’s idealized MOND limit with $f_b = 0.8$ (solid purple line), and from SFDM with $f_b = 0.8$ with the superfluid’s gravitational pull removed using two different methods. The first method is to set $\rho_{SF} = 0$ in SFDM’s equations (dotted green line). The second method is to keep ρ_{SF} , but use only the baryonic Newtonian acceleration when calculating the rotation curve (dash-dotted red line).

rotation curve. Indeed, the shape of the rotation curve is now closer to the rotation curve obtained using the ν_e interpolation function in McGaugh (2019). This becomes clear from Fig. 4 which compares the rotation curve for SFDM with $f_b = 0.8$ (dashed orange line), the rotation curve obtained using the ν_e interpolation function with $f_b = 1$ (solid blue line), and the rotation curve obtained in SFDM’s idealized MOND-limit for $f_b = 0.8$ (solid purple line).

This change of shape is due to the superfluid’s gravitational pull as one can see by removing the superfluid’s gravitational pull from the full SFDM model. The resulting rotation curves are very close to the rotation curve of SFDM’s idealized MOND-limit, as shown in Fig. 4. For this, we have tried two different methods of removing the superfluid’s gravitational pull from the full SFDM model, but both give similar results.

The first method is to simply set $\rho_{SF} = 0$. However, this does not just remove the superfluid’s gravitational pull but also influences the θ equation of motion, i.e. the equation that determines the phonon force. This is because $\hat{\mu}$ enters the θ equation of motion, but $\hat{\mu}$ is different with $\rho_{SF} = 0$ and $\rho_{SF} \neq 0$.

This motivates the second method of removing the superfluid’s gravitational pull for which we solve the full SFDM-equations without removing ρ_{SF} , but when calculating the rotation curve we take $\vec{\nabla}\phi_N$ to be only the baryonic Newtonian gravitational pull, not the full Newtonian gravitational force including ρ_{SF} . This method is more ad-hoc, but has the advantage that the solution for θ is not affected.

However, as one sees in Fig. 4, the difference between both methods is small. Both methods give a rotation curve that is very close to that of the idealized MOND-limit. Therefore, we can unambiguously attribute the shape differ-

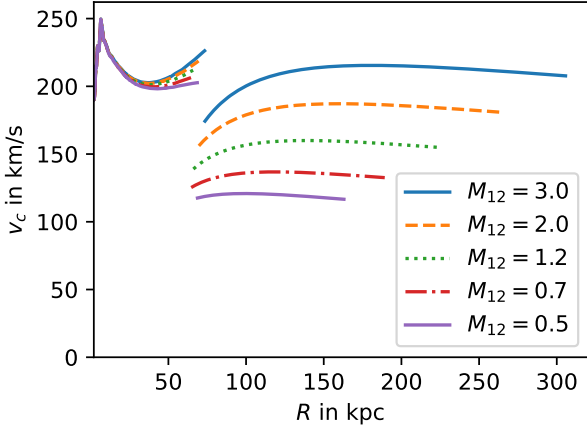


Figure 5. The rotation curves for different boundary conditions, corresponding to different total dark matter masses $M_{200}^{\text{DM}} \equiv M_{12} \cdot 10^{12} M_{\odot}$. Each rotation curve is plotted for $R < r_{200}$ with the virial radius r_{200} . M_{200}^{DM} and r_{200} are calculated assuming the NFW radius as the transition radius. The discontinuity at $R = R_{\text{NFW}}$ is because we assume the phonon force is switched off at this radius. See also Table 2.

Table 2. The results of the calculation of the NFW radius R_{NFW} , the total dark matter mass M_{200}^{DM} , the virial radius r_{200} , and the thermal radius R_T for various boundary conditions μ_{∞} imposed at a radius r_{∞} . M_{200}^{DM} and r_{200} are calculated assuming the NFW radius as the transition radius. The baryonic density is kept fixed with $f_b = 0.8$.

r_{∞} kpc	μ_{∞}/m 10^{-8}	R_{NFW} kpc	M_{200}^{DM} $10^{12} M_{\odot}$	r_{200} kpc	R_T kpc
110	7.80	73	3.0	306	105
100	6.24	70	2.0	265	97
100	1.25	66	1.2	225	87
90	0.25	65	0.7	189	76
80	0.12	69	0.5	163	67

ence between the full model and the idealized MOND-limit to the superfluid's gravitational pull.

5.3 The Size of the Superfluid Core

In SFDM, galaxies contain a superfluid phase only at the centers of galaxies. In the outer parts of galaxies, the superfluid breaks down. The equations used above are valid only in the superfluid phase. Therefore, our results regarding the MW's rotation curve are valid only if the superfluid phase extends to $R > 25$ kpc. To check that it is consistent to use only the superfluid phase to fit the rotation curve data, we therefore estimated the size of the MW's superfluid core using the methods outlined in 4.2.

For $f_b = 0.8$, we found the thermal radius to be $R_{T,R} = 87.5$ kpc and $R_{T,z} = 87.6$ kpc. Thus, the superfluid's thermal radius is almost the same in R - and z -direction. This is not surprising since we assumed spherical symmetry at large radii. Also, $R_{T,R}$ is much larger than 25 kpc. This indicates

that our above procedure for calculating the rotation curve is justified.

For $f_b = 0.8$, we found the NFW radius to be $R_{\text{NFW},R} = 66.0$ kpc and $R_{\text{NFW},z} = 65.7$ kpc. Thus, the superfluid seems to be sufficiently spherically symmetric at the NFW radius for our procedure to make sense. Just as the thermal radius $R_{T,R}$, the NFW radius $R_{\text{NFW},R}$ is much larger than 25 kpc indicating that our above procedure for calculating the rotation curve is justified.

The difference between the NFW and the thermal radii is about 30 %, similar to the NFW and thermal radii of the spherically symmetric galaxies studied in Berezghiani et al. (2018). Therefore, we should take these radii as rough estimates rather than precise values, as discussed in Berezghiani & Khoury (2015); Berezghiani et al. (2018). This is a limitation of this approach which assumes all of the dark matter particles to be in the condensed, superfluid phase in the inner parts of a galaxy with a sharp transition to the non-condensed, normal phase at larger radii. It may be possible to improve on this using a two-component approach where one component is in the superfluid phase and one component is in the normal, not-condensed phase. Nevertheless, the above suggests that the NFW and thermal radii give a reasonable first approximation for the transition also in non-spherically-symmetric galaxies.

5.4 Estimates for the total dark matter mass

So far, we used a fixed boundary condition $\mu_{\infty}/m = 1.25 \cdot 10^{-8}$ at $r_{\infty} = 100$ kpc. The reason is that the rotation curve at $R < 25$ kpc depends only very weakly on this boundary condition. However, the same is not true for the size of the superfluid core and the dark matter profile outside this superfluid core. A similar observation was previously discussed in Secs. 6.2 and 6.3 of Hossenfelder & Mistele (2018). Therefore, we here use several different boundary conditions to illustrate the behavior of SFDM on larger scales. For each choice of boundary condition, we estimate the thermal radius, the NFW radius, the total dark matter mass, and the virial radius. To keep a reasonable fit to the rotation curve at $R < 25$ kpc, we fix $f_b = 0.8$.

Following Berezghiani et al. (2018), we assume that the NFW halo is matched to the superfluid core at the NFW radius R_{NFW} . For concreteness, we take $R_{\text{NFW}} \equiv R_{\text{NFW},R}$.

To estimate the virial radius and the total mass of dark matter in both the superfluid and normal phase, we use the density profile given by ρ_{SF} for $r < R_{\text{NFW}}$ and the NFW profile ρ_{NFW} matched at $r = R_{\text{NFW}}$ for $r > R_{\text{NFW}}$. With this, we can calculate the virial mass as

$$M_{200}^{\text{DM}} = 2\pi \iint_{R^2+z^2 < R_{\text{NFW}}^2} dR R dz \rho_{\text{SF}}(R, z) + 4\pi \int_{R_{\text{NFW}}}^{r_{200}} dr r^2 \rho_{\text{NFW}}(r). \quad (12)$$

Here, r_{200} is the spherical radius where the mean dark matter density drops below $200 \cdot 3H^2/(8\pi G)$, where H is the Hubble constant. Here, we use $H = 67.3$ km/(s · Mpc).

We choose a set of boundary conditions that covers a range in M_{200}^{DM} from $0.5 \cdot 10^{12} M_{\odot}$ to $3 \cdot 10^{12} M_{\odot}$. This covers the range of measured values given in Bland-Hawthorn

& Gerhard (2016)². The precise boundary conditions and results are given in Table 2. For each boundary condition, we show the corresponding rotation curve up to the virial radius in Fig. 5.

The rotation curves have discontinuities at $R = R_{\text{NFW}}$ because in the model of (Berezhiani & Khoury 2015; Berezhiani et al. 2018) the phonon force is assumed to be effective only inside the superfluid core. Therefore, we include this force only for $R < R_{\text{NFW}}$. In a real galaxy, of course, this transition should be gradual and not abrupt. How exactly this transition happens requires further theoretical work that is beyond the scope of the present paper. Thus, the rotation curves shown in Fig. 5 should not be taken too seriously around the discontinuity at $R = R_{\text{NFW}}$. Away from this discontinuity the rotation curves should represent the SFDM expectation.

As one sees from Fig. 5, the rotation curves agree with each other for small radii, but deviate at larger radii, where the difference in the boundary conditions becomes important. We also see that the rotation curves bend upwards before $R = R_{\text{NFW}}$. This is due to the combination of the phonon force, which gives flat rotation curves, and the cored superfluid dark matter profile which starts to contribute significantly to the rotation curve at these radii. This was already observed in Berezhiani et al. (2018). This effect increases with increasing M_{200}^{DM} which may rule out larger values of M_{200}^{DM} .

A glance at Table 2 makes clear that the thermal radius depends more strongly on the boundary conditions than the NFW radius. The NFW radius varies from 65 kpc for $M_{200}^{\text{DM}} = 0.7 \cdot 10^{12} M_{\odot}$ to 73 kpc for $M_{200}^{\text{DM}} = 3 \cdot 10^{12} M_{\odot}$, while the thermal radius varies from 67 kpc for $M_{200}^{\text{DM}} = 0.5 \cdot 10^{12} M_{\odot}$ to 105 kpc for $M_{200}^{\text{DM}} = 3 \cdot 10^{12} M_{\odot}$. Still, for the range of parameters considered here, the thermal radius and the NFW radius agree with each other to roughly 30 % as in Berezhiani et al. (2018).

We find that the virial radius r_{200} varies from 163 kpc for $M_{200}^{\text{DM}} = 0.5 \cdot 10^{12} M_{\odot}$ to 306 kpc for $M_{200}^{\text{DM}} = 3 \cdot 10^{12} M_{\odot}$. Assuming M31 to have a roughly similar virial radius, these values indicate that, today, there is no overlap of the halos of MW and M31, since the distance to M31 is about 770 kpc (Karachentsev et al. 2004). However, for even larger MW (or M31) masses, their halos may overlap so that dynamical friction may become important.

6 DISCUSSION

In this present work, we are concerned with the rotation curve at $R < 25$ kpc. In this range, the rotation curve depends only weakly on μ_{∞} . It then suffices to confirm that our choice of μ_{∞} gives a superfluid core extending to $R > 25$ kpc as well as a reasonable rotation curve. As discussed in the previous section, this is indeed the case. The precise choice of μ_{∞} , however, becomes important for comparison to data at larger radii, especially beyond the superfluid core. For example, we saw explicitly that the total dark matter mass and the virial radius depend strongly on this choice.

² Although it should be kept in mind that these measurements may not apply directly in SFDM if they assume standard CDM.

Knowing the transition radius and the behavior of SFDM at larger radii is important to predict the behavior of tracers of the gravitational potential at these larger radii. For example, as discussed in Berezhiani et al. (2018), tidal stellar streams may exhibit peculiar features due to crossing the transition radius. The present work can be a first step towards making predictions for such features. Similarly, the transition radius determines which satellite galaxies and globular clusters are affected by a MOND-like External Field Effect (EFE) (Milgrom 1983a; Famaey & McGaugh 2012), since a MOND-like EFE applies only inside the superfluid core in SFDM (Berezhiani et al. 2018).

It must further be mentioned that while we compared the model of SFDM to rotation curve data, in the Milky Way this is not the only available data. For example, there may be additional constraints from vertical acceleration measurements as discussed in Lisanti et al. (2019b,a). These constraints are a serious problem for MOND. However, for SFDM they are not necessarily problematic. Because the superfluid interacts with the baryons, it should strictly speaking also rotate, which quite plausibly affects the vertical gradient of the phonon-force. However, we do not presently have a theoretical framework to handle a rotating two-component fluid in a gravitational potential, so, unfortunately, we cannot address this interesting constraint here.

Above, we adjusted the parameter f_b to give a reasonable Milky Way rotation curve. For a proper statistical analysis, both the parameters of the baryonic mass distribution and the parameters of the SFDM model should be fitted. There is little reason to doubt that it is possible to obtain a good fit to the Milky Way rotation curve in this way because the model has four free parameters, whereas we were able to get a reasonable rotation curve with only one free parameter. However, attempting to fit the SFDM parameters to the MW rotation curve makes no sense in isolation because changing the parameters will affect the goodness-of-fit to other astrophysical data. To address this point, one would need to do a global fit to all available data to identify the best-fit parameters, but this is beyond the scope of this present work.

7 CONCLUSIONS

We have shown here that superfluid dark matter which mimics MOND with a phonon-force has no trouble explaining the newest data for the Milky-Way rotation curve. Superfluid dark matter provides a fit of the rotation curve that is similarly good as MOND, provided that the total baryonic mass is 10 – 20% less than the current estimates of the stellar mass. This amount of baryonic mass in the Milky Way is currently within measurement uncertainty. However, in the future, with better measurements of the Milky-Way’s baryonic mass, the here presented result may enable us to tell apart superfluid dark matter from MOND.

We have further demonstrated that the superfluid core’s size in axisymmetric galaxies can be estimated with a similar procedure as in spherically symmetric galaxies and we have calculated the total dark matter masses and virial radii for various boundary conditions. This can be an important first step to understand how satellite galaxies, globular clusters, and tidal stellar streams behave in SFDM.

ACKNOWLEDGEMENTS

We thank Stacy McGaugh for helpful discussion and for kindly providing the data used in our analysis. SH gratefully acknowledges support from the German Research Foundation (DFG). We also wish to thank an anonymous referee for helpful suggestions for improvement.

DATA AVAILABILITY

The data underlying this article will be shared on reasonable request to the corresponding author.

REFERENCES

- Abbott B. P., et al., 2017, *Astrophys. J.*, 848, L12
 Aguirre A., Diez-Tejedor A., 2016, *JCAP*, 1604, 019
 Bekenstein J. D., 2004, *Phys. Rev. D*, 70, 083509
 Bekenstein J., Milgrom M., 1984, *Astrophys. J.*, 286, 7
 Berezhiani L., Khoury J., 2015, *Phys. Rev.*, D92, 103510
 Berezhiani L., Famaey B., Khoury J., 2018, *JCAP*, 1809, 021
 Blanchet L., Heisenberg L., 2015, *J. Cosmology Astropart. Phys.*, 2015, 026
 Bland-Hawthorn J., Gerhard O., 2016, *ARA&A*, 54, 529
 Bovy J., Rix H.-W., 2013, *Astrophys. J.*, 779, 115
 Brada R., Milgrom M., 1995, *Monthly Notices of the Royal Astronomical Society*, 276, 453
 Davidson S., 2015, *Astropart. Phys.*, 65, 101
 Davidson S., Elmer M., 2013, *JCAP*, 1312, 034
 Deffayet C., Esposito-Farèse G., Woodard R. P., 2011, *Phys. Rev. D*, 84, 124054
 Dev P. S. B., Lindner M., Ohmer S., 2017, *Phys. Lett.*, B773, 219
 Eby J., Ma M., Suranyi P., Wijewardhana L. C. R., 2018, *JHEP*, 01, 066
 Eilers A.-C., Hogg D. W., Rix H.-W., Ness M. K., 2019, *Astrophys. J.*, 871, 120
 Famaey B., McGaugh S. S., 2012, *Living Reviews in Relativity*, 15, 10
 Freeman K. C., 1970, *Astrophys. J.*, 160, 811
 Gravity Collaboration 2018, *A & A*, 615, L15
 Gravity Collaboration et al., 2019, *A&A*, 625, L10
 Guth A. H., Hertzberg M. P., Prescod-Weinstein C., 2015, *Phys. Rev.*, D92, 103513
 Hossenfelder S., 2017, *Phys. Rev.*, D95, 124018
 Hossenfelder S., Mistelet T., 2018, *International Journal of Modern Physics D*, 27, 1847010
 Hossenfelder S., Mistelet T., 2019, *JCAP*, 1902, 001
 Karachentsev I. D., Karachentseva V. E., Huchtmeier W. K., Makarov D. I., 2004, *AJ*, 127, 2031
 Lelli F., McGaugh S. S., Schombert J. M., Pawlowski M. S., 2017, *Astrophys. J.*, 836, 152
 Licquia T. C., Newman J. A., 2015, *Astrophys. J.*, 806, 96
 Lisanti M., Moschella M., Outmezguine N. J., Slone O., 2019a, arXiv e-prints, p. arXiv:1911.12365
 Lisanti M., Moschella M., Outmezguine N. J., Slone O., 2019b, *Phys. Rev. D*, 100, 083009
 McGaugh S. S., 2008, *Astrophys. J.*, 683, 137
 McGaugh S., 2019, *Astrophys. J.*, 885, 87
 McMillan P. J., 2017, *Monthly Notices of the Royal Astronomical Society*, 465, 76
 Milgrom M., 1983a, *Astrophys. J.*, 270, 365
 Milgrom M., 1983b, *Astrophys. J.*, 270, 384
 Milgrom M., 1986, *Astrophys. J.*, 302, 617
 Milgrom M., 2009, *Phys. Rev. D*, 80, 123536
 Milgrom M., 2010, *MNRAS*, 403, 886

- Noumi T., Saikawa K., Sato R., Yamaguchi M., 2014, *Phys. Rev.*, D89, 065012
 Olling R. P., Merrifield M. R., 2001, *Monthly Notices of the Royal Astronomical Society*, 326, 164
 Portail M., Gerhard O., Wegg C., Ness M., 2017, *Monthly Notices of the Royal Astronomical Society*, 465, 1621
 Sanders R. H., McGaugh S. S., 2002, *ARA&A*, 40, 263
 Sarkar S., Vaz C., Wijewardhana L. C. R., 2018, *Phys. Rev.*, D97, 103022
 Sikivie P., Yang Q., 2009, *Phys. Rev. Lett.*, 103, 111301
 Skordis C., Zlosnik T., 2020, arXiv e-prints, p. arXiv:2007.00082
 Wolfram Research, Inc. 2019, Mathematica, Version 12
 Zlosnik T. G., Ferreira P. G., Starkman G. D., 2007, *Phys. Rev. D*, 75, 044017
 de Vega H. J., Sanchez N. G., 2014

APPENDIX A: NUMERICAL METHOD

To numerically solve the equations summarized in Section 2, we run Mathematica 12's (Wolfram Research, Inc. 2019) PDESolve in the region $R^2 + z^2 < r_\infty^2$, $z > 0$ with $r_\infty = 100$ kpc, unless stated otherwise. The value of r_∞ is chosen such that it is much larger than the size of the stellar and gas disks. It is possible to solve the equations only in the region $z > 0$ because in our approximation the Milky Way is symmetric under $z \rightarrow -z$.

The Mathematica function PDESolve operates on a triangulation of the region described above. For this, we impose the following maximum areas of the triangular cells: For $R < 20$ kpc and $z < 0.5$ kpc, the maximum area is $(0.05 \text{ kpc})^2$. For $R < 40$ kpc and $z < 5$ kpc, it is $(0.2 \text{ kpc})^2$. For $R < 40$ kpc and $z < 10$ kpc, it is $(1 \text{ kpc})^2$. For $R < 40$ kpc and $z < 20$ kpc, it is $(2 \text{ kpc})^2$. Otherwise, the maximum area is $(10 \text{ kpc})^2$.

In the term of the form $\vec{\nabla}(g \vec{\nabla} \theta)$, g is not a smooth function for $\theta, \hat{\mu} \rightarrow 0$ due to the square roots in g . Unfortunately, this causes Mathematica's PDESolve to fail with the error "NDSolve::femdpop: The FEMStiffnessElements operator failed." We work around this as follows. In the case of the full SFDM model, we rewrite the model, including the boundary conditions, in terms of $\hat{\mu}_{\text{temp}}(R, z) = \hat{\mu}(R, z) + \Delta\hat{\mu}$, where $\Delta\hat{\mu}$ is a constant. This suffices to make PDESolve solve the equations in terms of $\hat{\mu}_{\text{temp}}$. The solution for $\hat{\mu}_{\text{temp}}$ then gives a solution for $\hat{\mu}$ by subtracting $\Delta\hat{\mu}$. We verified that our results do not depend on the choice of $\Delta\hat{\mu}$. In the case of the idealized MOND limit, we simply shift $\sqrt{(\vec{\nabla} \bar{\theta})^2} \rightarrow \sqrt{C + (\vec{\nabla} \bar{\theta})^2}$ with a constant $C \ll (\vec{\nabla} \bar{\theta})^2$. We verified that $C \ll (\vec{\nabla} \bar{\theta})^2$ for the obtained solutions and that the choice of C does not affect our results.

This paper has been typeset from a \LaTeX file prepared by the author.